Draft version November 16, 2016
Preprint typeset using LaTeX style AASTeX6 v. 1.0

arXiv:1611.04659v1 [astro-ph.SR] 15 Nov 2016

THE RADIAL DISTRIBUTIONS OF THE TWO MAIN-SEQUENCE COMPONENTS IN THE YOUNG MASSIVE STAR CLUSTER NGC 1856

Chengyuan Li[1], Richard de Grijs[2,3], Licai Deng[4], Antonino P. Milone[5]
[1]Department of Physics and Astronomy, Macquarie University, Sydney, NSW 2109, Australia

[2]Kavli Institute for Astronomy & Astrophysics and Department of Astronomy, Peking University, Yi He Yuan Lu 5, Hai Dian District, Beijing 100871, China

[3]International Space Science Institute–Beijing, 1 Nanertiao, Zhongguancun, Hai Dian District, Beijing 100190, China

[4]Key Laboratory for Optical Astronomy, National Astronomical Observatories, Chinese Academy of Sciences, 20A Datun Road, Chaoyang District, Beijing 100012, China

and

[5]Research School of Astronomy & Astrophysics, Australian National University, Mt Stromlo Observatory, Cotter Rd, Weston, ACT 2611, Australia

ABSTRACT

The recent discovery of double main sequences in the young, massive star cluster NGC 1856 has caught significant attention. The observations can be explained by invoking two stellar generations with different ages and metallicities or by a single generation of stars composed of two populations characterized by different rotation rates. We analyzed the number ratios of stars belonging to both main-sequence components in NGC 1856 as a function of radius. We found that their number ratios remain approximately unchanged from the cluster's central region to its periphery, indicating that both components are homogeneously distributed in space. Through a comparison of the loci of the best-fitting isochrones with the ridge lines of both stellar components, we found that both multiple stellar populations and rapid stellar rotation can potentially explain the observed main-sequence bifurcation in NGC 1856. However, if NGC1856 were a young representative of the old globular clusters, then the multiple stellar populations model would not be able to explain the observed homogeneity in the spatial distributions of these two components, since all relevant scenarios would predict that the second stellar generation should be formed in a more compact configuration than that of the first stellar generation, while NGC 1856 is too young for both stellar generations to have been fully mixed dynamically. We speculate that the rapid stellar rotation scenario would be the favored explanation of the observed multiple stellar sequences in NGC 1856.

Keywords: globular clusters: individual: NGC1856 – Hertzsprung-Russell and C-M diagrams – Magellanic Clouds

1. INTRODUCTION

Current consensus on the formation of star clusters suggests that a cluster's initial star-formation process approximately resembles a single burst (Longmore et al. 2014). However, the discovery of ubiquitous multiple stellar populations in globular clusters (GCs) (e.g., Carretta et al. 2009; Milone et al. 2012; Piotto et al. 2015), as well as the extended main-sequence turn-offs (eMSTOs) in most intermediate-age star clusters (e.g., Milone et al. 2009; Girardi et al. 2013) has strongly challenged this notion. The nature of the eMSTOs in intermediate-age star clusters is still

chengyuan.li@mq.edu.au

being debated (Li et al. 2014a; Bastian & Niederhofer 2015; Goudfrooij et al. 2015; Bastian et al. 2016). The multiple stellar populations in GCs exhibit significantly different chemical abundances (e.g., Kraft 1979; Carretta et al. 2009), which is in strong conflict with the expectations from the formation scenario of coeval stellar populations. For example, Milone et al. (2012) found two distinct main sequences (MSs) in the GC 47 Tucanae (47 Tuc), which can be explained by CN-weak/O-rich/Na-poor/He-poor and CN-strong/O-poor/Na-rich-He-rich populations. The latter has been speculated to represent a second stellar generation, which may have originated from material whose metallicity had been enhanced by the waste products of the first-generation stars. In addition, di Criscienzo et al. (2010) studied the morphology of MS, horizontal-branch (HB) and subgiant branch (SGB) stars in 47 Tuc using population synthesis. They concluded that 47 Tuc may also possess a spread in helium abundance in its more evolved stars (for confirmation, see Nataf et al. 2011). Similar results have been also found for the GC NGC 2808, which shows triple MSs that can be explained by three stellar populations with different helium abundances (Piotto et al. 2015). Some GCs, including NGC 1851 and NGC 6656, exhibit split subgiant branches (SGBs) in optical filters which correspond to stellar populations containing different amounts of heavy elements (see Marino et al. 2015, and references in their Table 10). In addition, the red-giant branches (RGBs) in most GCs are split into multiple components, especially when ultraviolet (UV) observations are used (e.g., Piotto et al. 2015).

Based on accurate photometry, marked differences in the dynamics of different stellar populations have also been found in many GCs. Milone et al. (2012) found that the second stellar generation in 47 Tuc (the CN-strong/O-poor/Na-rich population) has a higher central concentration than the first stellar generation, a result that was confirmed by Li et al. (2014b). Massari et al. (2016) found two well-populated RGBs in the GC M3 (NGC 5272), which can be explained by an N-poor/Na-poor first stellar generation and an N-rich/Na-rich second stellar generation. The second-generation stars are significantly more centrally concentrated than the cluster's first-generation stars. Lardo et al. (2011) analyzed seven Galactic GCs based on Sloan Digital Sky Survey (SDSS) photometric data. They found that all UV–red RGBs in these GCs are more centrally concentrated than their UV–blue counterparts, where the UV–red RGB stars are mainly composed of Na-rich stars, i.e., those stars that should belong to the second stellar generation.

Numerous scenarios have been proposed to explain the multiple stellar populations in GCs. Most of these draw on self-pollution of the intra-cluster gas (Li et al. 2016). The polluters that may explain the enriched secondary stellar generations are diverse, including rapidly rotating massive stars (Decressin et al. 2007), massive binaries (de Mink et al. 2009), and evolved post-giant-branch stars (Ventura & D'Antona 2009). However, most of these scenarios are still associated with sometimes severe problems (e.g., Renzini et al. 2015; Bastian et al. 2015). All of these scenarios predict that the second stellar generation should formed in a more concentrated configuration compared with a cluster's first stellar generation (Renzini 2008; Vesperini et al. 2013; Hénault-Brunet et al. 2015; Khalaj & Baumgardt 2015).

The first evidence of possible multiple stellar populations in young clusters was discovered in the Large Magellanic Cloud (LMC) cluster NGC 1856 (Correnti et al. 2015; Milone et al. 2015). It shows an apparent eMSTO, and its MS splits into two distinct components, which cannot be explained by a coeval, chemically homogeneous stellar population. Similar discoveries for other young, massive clusters (YMCs) followed: Bastian et al. (2016) found that the MSTO region of the YMC NGC 1850 is significantly more extended than predicted for simple stellar populations. Similarly to NGC 1856, it was found that the YMC NGC 1755 also exhibits an apparent bifurcation in its MS (Milone et al. 2016).

Although there is growing evidence of the reality of multiple stellar populations in YMCs, the dynamics of these different stellar populations are still poorly understood. In this paper, we analyze the radial profile of the number ratio of the two MS components in NGC 1856. We find that both stellar sequences are not very different in terms of their spatial distributions. The number ratio of the two components as a function of radius remains constant. Two equally likely scenarios could potentially explain the observed multiple MS components in NGC 1856: the observed multiple sequences can be explained by either invoking multiple stellar populations of different ages and metallicities, or a coeval stellar population characterized by member stars that exhibit two different rotation rates (D'Antona et al. 2015). However, if the former explanation were correct, and if NGC 1856 is indeed the infant stage of an old GC, the second-generation stars should be initially more centrally concentrated than their first-generation counterparts (Renzini 2008; Vesperini et al. 2013; Hénault-Brunet et al. 2015; Khalaj & Baumgardt 2015). Since NGC 1856 is very young ($\sim$300 Myr; Milone et al. 2015), this difference in their radial distributions should be still apparent, but this prediction is in conflict with our observations. Our result may indicate that the observed multiple stellar sequences in NGC 1856 have actually been produced by a coeval stellar population composed of two components of stars with different rotation rates. However, we emphasize that it is still unclear whether the stellar components characterized by different rotation rates would be different in their spatial distributions; follow-up research to explore this aspect is required.

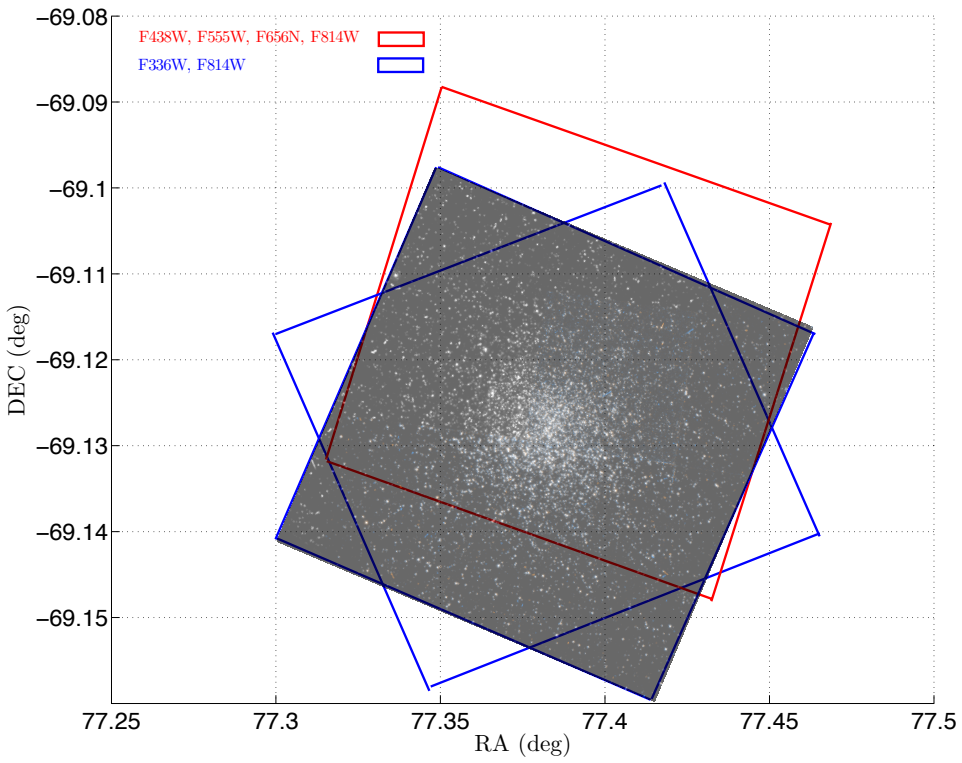

Figure 1. Footprints of the NGC 1856 fields. The fields for the F438W, F555W, F656N, and F814W observations are based on *HST* program GO-13011 (red box); the images in the F336W and F814W filters (blue boxes) are from *HST* program GO-13379. For more details, see Table 1 of Milone et al. (2015). The true-color image (http://www.wikiwand.com/en/NGC_1856) clearly shows the outlines of the observational fields with respect to the position of the cluster.

This article is arranged as follows. Section 2 describes our data reduction. Section 3 contains the main results of our analysis. In Section 4 we discuss the possible underlying physics that may produce the observed results. Section 5 includes our conclusions.

2. DATA REDUCTION

We used the photometric catalogs of Milone et al. (2015), based on observations with the *Hubble Space Telescope* (*HST*) using the Ultraviolet and Visual channels of the Wide Field Camera 3 (UVIS/WFC3). The data sets used here, which were observed through the F336W and F438W filters, were obtained as part of the observational programs GO-13011 (PI: T. H. Puzia) and GO-13379 (PI: A. P. Milone).[1] Relevant information pertaining to our data set is summarized in Table 1 of Milone et al. (2015). Figure 1 shows the footprints of the observational fields. The resulting stellar catalog is based on accurate point-spread-function photometry using a software program developed by Anderson et al. (2008). Both the zero points and the differential reddening are well calibrated (for more details, see Milone et al. 2015).

The first step involves the determination of the cluster center coordinates. Because we will focus on the number ratio of the two main-sequence components, using the location where the stellar number density reaches its maximum as cluster center is appropriate. The method we used to determine the stellar number density center in NGC 1856 is identical to that of Li et al. (2016): we first divided all stars into 20 bins along both the right ascension ($\alpha_{\rm J2000}$) and declination ($\delta_{\rm J2000}$) axes. We then used a Gaussion function to fit their number density distribution along both axes. The resulting peaks of the best-fitting Gaussian function in each direction thus represent the coordinates of the cluster center, ($\alpha_{\rm J2000} = 05^{\rm h}09^{\rm m}31.34^{\rm s}$, $\delta_{\rm J2000} = -69°07'42.07''$). Our result is consistent with the center coordinates

[1] The complete data sets include five bands, i.e., F336W, F438W, F555W, F656N, and F814W: see Fig. 1. In this paper, we only use the observations in the F336W and F438W bands, because the MS bifurcation in NGC 1856 is most apparent in (F336W, F336W–F438W) color–magnitude space.

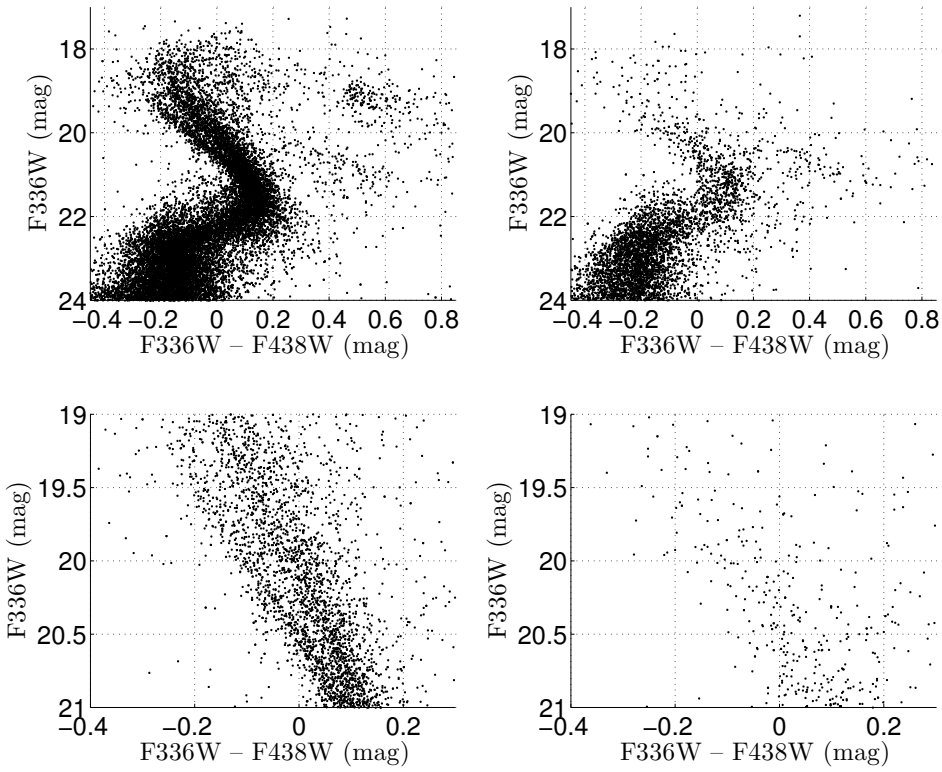

Figure 2. (top left) NGC 1856 CMD. (top right) CMD of the reference field. (bottom) As the top panels, but highlighting the magnitude range 19 ≤ F336W ≤ 21 mag.

of Werchan & Zaritsky (2011).

We next need to define an appropriate cluster size. We calculated the angular distances to the adopted cluster center for all stars in the catalog. We divided the observed field into 20 concentric rings, with radii spanning from 10″ to 105″. We then calculated the average stellar number densities for these 20 rings. This procedure provided us with a monotonically decreasing number density profile of the stars in NGC 1856. We simply define the radius where the stellar number density decreases to about half the central density (the density within $R = 10''$) as the 'core' size, $R_c = 22.5''$. We used the region at radii in excess of four times the core size ($R \geq 90''$) to evaluate the corresponding average number density. Since this region is located far from the cluster center, we treat its average number density as the 'field' level. The radius where the cluster's stellar number density disappears into the field's stellar population is defined as the cluster size, $R \approx 70''$ or about three core radii. We subsequently selected the region with $R \geq 75''$ as our reference field, which will be used for background correction. Using a Monte Carlo-based approach, we determined that the area of the cluster region is about 2.3 times larger than that of the referenced field. In Fig. 2, we present the raw (F336W, F336W–F438W) color–magnitude diagram (CMD) of the cluster region (left panels) as well as that of the reference field (right panels). An apparent split in the cluster's MS is found for 19 ≤ F336W ≤ 21 mag, which is shown in the bottom left-hand panel of Fig. 2.

Finally, we calculated the ridge lines describing both MS components. For both components, we connected the maximum number-density points across the range 19 ≤ F336W ≤ 21 mag. The resulting ridge lines are shown in Fig. 3. We then explored the dispersions associated with these ridge lines. We used an exponential function to fit the relationship between the stellar magnitudes and their corresponding photometric uncertainties, similar to that used by Li et al. (2013, their Fig. 4). Based on this empirical function, we defined the boundaries of the dispersion distributions corresponding to the 3σ (standard deviations) levels for both MS components. Finally, all stars with (a) color–magnitude loci between the blue and red boundaries (i.e., the blue and red dashed lines in Fig. 3) and (b) F336W magnitudes between 19.25 mag and 20.75 mag were selected as sample stars.

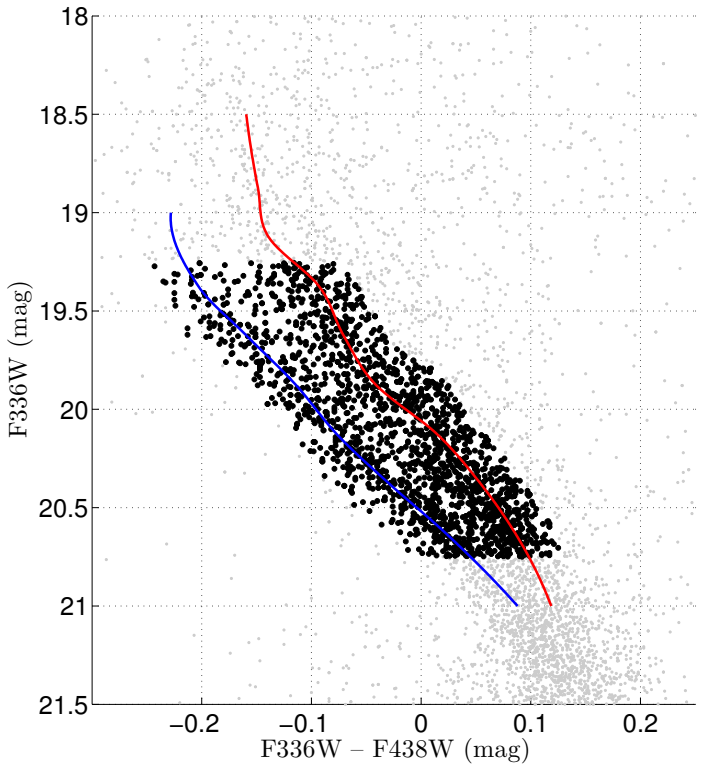

Figure 3. CMD of the region containing our sample stars: stars with magnitudes in the range 19.25 ≤ F336W ≤ 20.75 mag and colors between the 3σ boundaries of the blue and red ridge lines are part of our final sample (black dots).

3. MAIN RESULTS

Once we had defined the sample of MS stars, we evaluated the relative number ratio of stars belonging to both MS components. We used a similar method to that used in Fig. 1 of Milone et al. (2015): we projected both MS components along the vertical axis by defining a parameter $\Delta^N_{\rm F336W,F438W} = [(C - C_{\rm A})/(C_{\rm B} - C_{\rm A})]$ for each star, where $C = F336W - F4388W$ is the star's color and $C_{\rm A}, C_{\rm B}$ are the color residuals corresponding to ridge lines A and B, respectively. The same approach is also applied to stars belonging to the reference field. Contamination by field stars is subsequently reduced based on the $\Delta^N_{\rm F336W,F438W}$ distribution of the sample stars. Our resulting number distribution, $\Delta^N_{\rm F336W,F438W}$, shows two peaks. The distribution is well-described by two-component Gaussian functions,

$$N(\delta) = N_{\rm A}(\delta) + N_{\rm B}(\delta) = a_1 e^{-\left(\frac{\delta - b_1}{c_1}\right)^2} + a_2 e^{-\left(\frac{\delta - b_2}{c_2}\right)^2}, \quad (1)$$

where $N(\delta)$ is the number corresponding to a given value of $\Delta^N_{\rm F336W,F438W}$, and $N_{\rm A}$ and $N_{\rm B}$ are the contributions from the blue ('A' in Fig. 4) and red ('B' in Fig. 4) component stars. The relative number ratio of these two components can be represented by the ratio of the areas of their corresponding Gaussian functions,

$$f = \frac{N_{\rm A}}{N_{\rm B}} = \frac{\int_{-\infty}^{\infty} a_1 e^{-\left(\frac{\delta - b_1}{c_1}\right)^2} {\rm d}\delta}{\int_{-\infty}^{\infty} a_2 e^{-\left(\frac{\delta - b_2}{c_2}\right)^2} {\rm d}\delta} = \frac{\sqrt{\pi} a_1 c_1/2}{\sqrt{\pi} a_2 c_2/2} = \frac{a_1 c_1}{a_2 c_2}. \quad (2)$$

The resulting number ratio of stars associated with both components is $N_{\rm A}/N_{\rm B}$=34%/66%: see Fig. 4. The component-B stars dominate the stellar numbers (see also Milone et al. 2015, 33%/67%).

We next examined whether the two stellar components exhibited different spatial distributions. We first examined the cumulative profiles of the number distributions of both stellar components. We divided the sample into seven concentric circles with radii spanning from 10″ to 70″. For each annulus, we performed the same approach with the stars located at those radii. The cumulative number distributions of components A and B stars are presented in

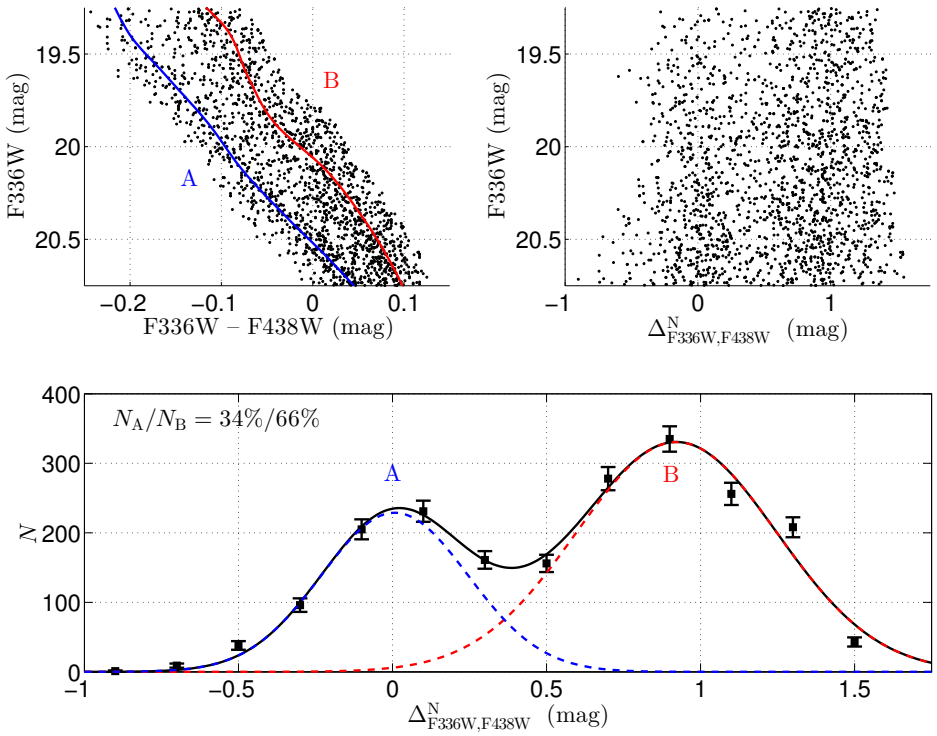

Figure 4. Illustration of our calculation of the number ratio of stars belonging to both MS components. The top left-hand panel shows the CMD of the two MS components and the adopted ridge lines (thick lines). The top right-hand panel shows the corresponding distributions of the stellar color deviations from these ridge lines. The best-fitting double Gaussian profile is shown in the bottom panel.

Fig. 5 (top panel). We found that in the 95% confidence range,[2], the profiles of the cumulative number distributions for component-A and -B stars are not significantly different. This is also reflected by the profile of their number ratio, N_A/N_B. The value of N_A/N_B for the entire cluster region ($10'' \leq R \leq 70''$) ranges from 43% to 51%, and the uncertainties corresponding to the 95% confidence interval range from ∼4% to 9%.

We also studied the annular N_A/N_B profile. We divided our sample into seven rings with boundaries at 10, 15, 20, 27, 35, and 45 arcsec. These boundaries were adopted to ensure that the stellar numbers in each ring were similar. As expected, the resulting N_A/N_B profile is highly dispersed compared with the cumulative profile (see the grey dashed line in the bottom panel of Fig. 5). The latter is smoother, because it contains a larger number of stars. However, the shape of the annular N_A/N_B profile is consistent with most details in the variations of the cumulative number ratio profile. For example, if the number ratio in a given ring is higher (lower) than the average value, the overall value of the cumulative number ratio at the corresponding radius increases (decreases) as well.

In summary, our results show that the radial distributions of stars in the two MS components are not very different. The cumulative profile of their number and the number ratio distributions do not change significantly with radius from the cluster's central region to its outskirts. The annular profile of the number ratio of the blue and red components, N_A/N_B, is also consistent with the cumulative profile.

4. DISCUSSION

4.1. *Binary Segregation?*

It is unlikely that unresolved binaries are responsible for the observed MS bifurcation. The color separation between both MS components in NGC 1856 reaches 0.1 mag or more. Such a large separation in color indicates that if the red-component stars are binary systems, they should be approximately equal-mass binaries (see Li et al. 2013, their

[2] In this paper, we simply adopt Poissonian dispersions for the numbers of stars in the different components.

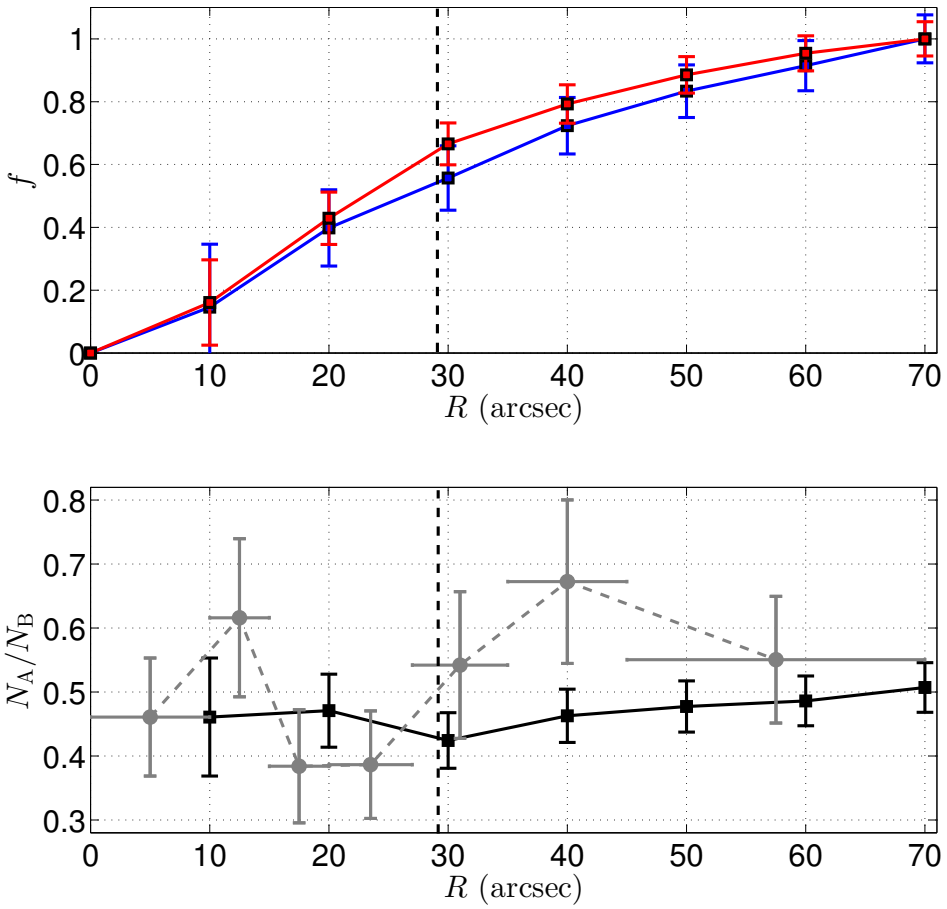

Figure 5. (Top) Cumulative number distributions of components A and B. (Bottom) Radial profile of the number ratio of components A and B (N_A/N_B. Black solid line: cumulative profile; grey dashed line: annular profile. The vertical black dashed lines (in both panels) indicate the half-light radius of NGC 1856 (McLaughlin & van der Marel 2005).

Fig. 9). However, because the red-component stars dominate the stellar numbers at a given magnitude, this means most binaries in NGC 1856 must be high mass-ratio binary systems. This, in turn, is in conflict with many previous studies (e.g., Kouwenhoven et al. 2005, 2007; Reggiani & Meyer 2011).[3] In addition, since binaries are more massive on average than single stars, binaries are usually more dynamically segregated (de Grijs et al. 2013) because of long-term two-body interactions (but see de Grijs et al. 2013; Li et al. 2013). If the observed double sequences in NGC 1856's CMD can be explained by single stars (blue sequence) and binaries (red sequence), stars that belong to the red MS component should be more segregated than the blue-population stars. This is in contrast to our results.[4]

4.2. *Multiple Star Forming Events?*

Two scenarios could potentially explain the MS split in the CMD of NGC 1856: (1) multiple stellar populations of different ages and metallicities or (2) a coeval stellar population composed of two stellar components that are distinctly different in terms of their rotation properties. We first explore the scenario pertaining to the presence of multiple stellar populations. If more than a single star-forming event had occurred, the second-generation stars should be characterized by enhancements of both their helium abundance and their metallicity. It is well-known that helium

[3] Note that these studies are based on explorations of stellar associations.

[4] It is also unlikely that the red-component stars are caused by line-of-sight blending. Using artificial star tests, we found that the blending fraction pertaining to our sample stars is only ∼2%, which cannot significantly change the resulting number-ratio profile. In addition, blending should cause the red-component stars to be apparently more centrally concentrated because of the high number density in the cluster's central region.

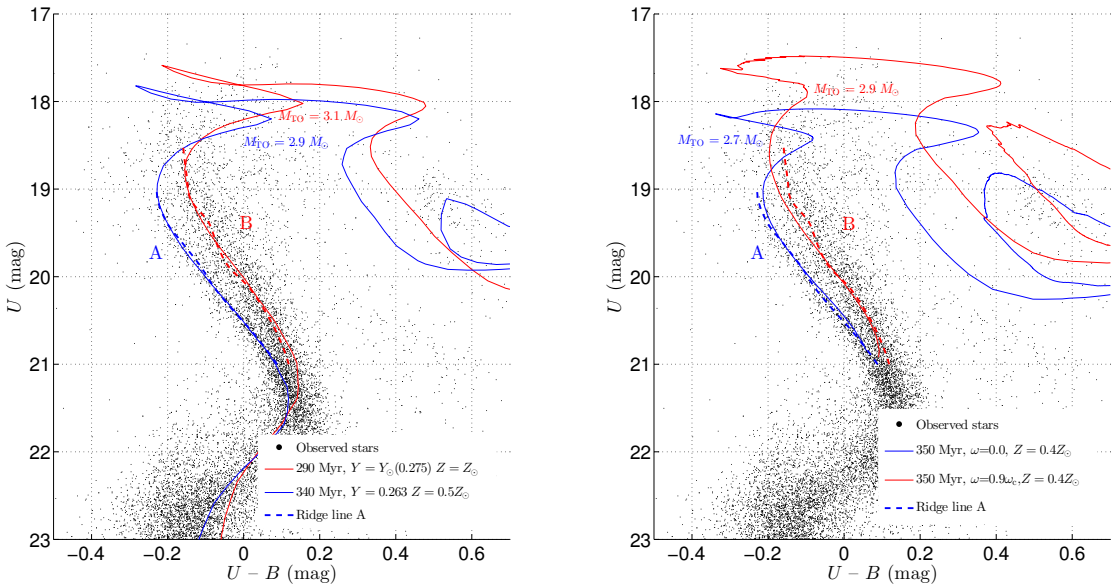

Figure 6. Isochrone fits to the two different MS components in NGC 1856. (left) Bressan et al. (2012) isochrones with different ages, helium abundances and metallicities, as indicated. (right) Both isochrones have the same age and metallicity, but they are characterized by different rotation rates (blue, red solid lines: non-rotating, rapidly rotating stars with $\omega = 0.9\omega_c$. These isochrones were calculated using the Geneva code (Ekström et al. 2012). The blue and red dashed lines are the ridge lines for both MS sequences. We have included the stellar masses of the turn-off (TO) stars in both panels. All stars studied in this paper are B- and early F-type stars.

variations are responsible for split MSs in old Galactic GCs, where the multiple sequences are usually well-described by isochrones with different helium abundances (e.g., Piotto et al. 2015). For young stellar clusters like NGC 1856, the MS regime studied in this paper is populated by very hot stars. In this regime of stellar gravity and temperature, the MSs of two stellar populations characterized by similar metallicities but different helium content are almost coincident. This is clearly shown in Fig. 9c of Milone et al. (2016), where two isochrones with very different helium abundances ($Y = 0.25$ and $Y = 0.40$) are compared with the observed CMD of NGC 1755. This figure clearly shows that helium differences cannot reproduce the large MS color split observed in NGC 1755, NGC 1856, and other young clusters in the Magellanic Clouds.

A more reasonable assumption is adoption of two stellar generations with different ages, helium abundances, and metallicities, where the younger-generation stars are both helium and metallicity enhanced. To test this idea, we generated a series of isochrones based on the Padova stellar evolution models (Bressan et al. 2012) for different ages and metallicities, with helium abundances defined by $Y = 0.2485 + 1.78Z$ (see Bressan et al. 2012, their Section 4). We determined the best-fitting isochrones to the observations by comparing their positions with the loci of the adopted ridge lines. We found that adopting isochrones that are only different in age (but identical in helium abundance and metallicity) cannot fit the positions of the two MS components.[5] Instead, to determine the best-fitting isochrones that most closely match the loci of the adopted ridge lines, we need to adopt isochrones that are different in both their ages and metallicities. That is, the young isochrone has a higher metallicity than the old isochrone. Finally, we determined an age of 290 Myr ($\log(t\ \mathrm{yr}^{-1}) = 8.46$) and a (solar) helium abundance and metallicity of $Y = 0.275$, $Z = 0.0152$ for the red MS component, while the best-fitting age and metallicity for the blue-component stars are 340 Myr ($\log(t\ \mathrm{yr}^{-1}) = 8.54$), $Y = 0.263$ and $Z = 0.008$ ($\sim 0.5Z_\odot$), respectively. The extinction and distance modulus adopted for both isochrones are $E(B-V) = 0.15$ mag and $(m-M)_0 = 18.35$ mag (cf. Milone et al. 2015, their Fig. 9). The fits resulting in isochrones with different ages and metallicities are shown in the left-hand panel of Fig. 6.

If our fits are indeed reliable, then these results indicate that the red stellar population is actually the second stellar generation, which formed more recently. This may further indicate that NGC 1856 could have retained the

[5] This approach is usually adopted to explain the eMSTO regions in most intermediate-age star clusters in the Magellanic Clouds (see, e.g., Milone et al. 2009).

initial runaway gas from supernova explosions, since the two observed stellar populations are different in their [Fe/H] abundances. The typical velocity of the runaway gas driven by Type II supernovae is on the order of 100 km s^{-1} (Rogers & Pittard 2013). If we assume that the half-mass radius of NGC 1856 is roughly equal to its half-light radius, $r_{\rm hl} = r_{\rm h} = 7.76$ pc (McLaughlin & van der Marel 2005), and that this also represents the initial half-light radius of NGC 1856, then the minimum mass for NGC1856 to retain the escaping gas driven by Type II supernovae is (Georgiev et al. 2009)

$$M_{\rm cl} \approx 100 v_{\rm esc}^2 r_{\rm h}. \quad (3)$$

Here we simply define $v_{\rm esc}$ ~100 km s^{-1}. Finally, we conclude that NGC 1856's initial mass should be *at least* $M_{\rm cl} \sim 7.76 \times 10^6 M_\odot$ to retain the runaway gas driven by Type II supernovae. The current mass of NGC 1856 is of order $10^5 M_\odot$ (McLaughlin & van der Marel 2005), while the enhanced metallicity of the second stellar generation in NGC 1856 would indicate that it has lost more than 99% of its initial mass during the last 340 Myr. It is difficult to explain how a cluster can lose such a large amount of mass during such a short period. This is equivalent to the so-called 'mass budget' problem that affects most scenarios that aim to explain the observed multiple stellar populations in GCs (Bastian et al. 2015) [6].

In addition, the observed homogeneity in the two stellar populations' spatial distributions is also different from that seen in most observed GCs, where the second stellar generation stars usually have a greater central concentration (Lardo et al. 2011; Milone et al. 2012; Massari et al. 2016). Our results would be in conflict with most scenarios that invoke the ejecta of the first-generation stars as the origin of any secondary stellar generations (Renzini 2008; Vesperini et al. 2013; Hénault-Brunet et al. 2015; Khalaj & Baumgardt 2015). All these scenarios predict that the secondary stellar generation stars should preferentially form in cluster's central region and thus have a higher concentration than the first-generation stars. However, a recent paper has shown revised spatial distributions for some subpopulations in the GCs NGC 362 and NGC 6723 (Lim et al. 2016), indicating that a higher concentration of second stellar generation stars may not necessarily be a common feature of GCs.

If the proposed multiple stellar population scenarios were on the right track, one possible explanation to the homogeneity in the spatial distributions of these two sequences is that they may initially have been different in terms of their radial distributions but were subsequently mixed through two-body relaxation. However, the half-mass relaxation timescale for stars in NGC 1856 is $t_{\rm hm} = 2.2$ Gyr (McLaughlin & van der Marel 2005), which is roughly seven times longer than the isochronal age of the cluster. This means that the observed spatial distributions of the two stellar populations should be close to their initial distributions, that is, they formed with uniform spatial distributions. However, all these speculations are based on the assumption that NGC 1856 is actually a young counterpart of the old GCs. It is also possible that the results from NGC 1856 cannot provide any constraints to the scenarios for multiple stellar populations in old GCs, given that all scenarios we have discussed deal with old GCs (Renzini 2008; Vesperini et al. 2013; Hénault-Brunet et al. 2015; Khalaj & Baumgardt 2015).

Based on all the considerations, we conclude that the MS bifurcation in NGC 1856 is most likely not caused by multiple stellar populations of different ages and metallicities.

4.3. *Rapid Stellar Rotation?*

D'Antona et al. (2015) explored the impact of rapid stellar rotation to explain the observed split in the MS of NGC 1856. They found that the observed CMD of NGC 1856 can be interpreted as a coeval stellar population composed of one-third of slowly/non-rotating stars and two-thirds of very rapidly rotating stars. We found that their conclusion is also valid for our (F336W, F336W–F438W) CMD: using the same isochrones as those adopted by D'Antona et al. (2015), we show the performance of our isochrone fits in the right-hand panel of Fig. 6. We found that the blue and red MS components can be well described by stellar populations characterized by a zero rotation rate ($\omega = 0$) and a level at 90% of the critical rotational rate ($\omega = 0.9\omega_{\rm c}$), respectively. This means that the number ratio of slowly/non-rotating and rapidly rotating stars is 39%/61% (see the bottom right-hand panel of Fig. 5), which is consistent with D'Antona et al. (2015).

It is unclear whether the slowly/non-rotating stars and their rapidly rotating counterparts in a star cluster should preferentially form at different locations. Thus far, no research has explored the relationship, if any, between stellar rotation rates and their spatial distributions. In our observations, the rapidly rotating stars are redder than the non/slowly rotating stars, indicating that the rapidly rotating stars are strongly affected by gravity darkening (Li et

[6] Note that Larsen et al. (2012) has estimated that the initial mass of GCs in the Fornax dwarf spheroidal galaxy would only need to be 4 – 5 times more massive than their current mass, on average.

al. 2016; Georgy et al. 2014). If gravity darkening is the *only* case that leads to an observed color difference such as that between our two populations, then this would indicate that the average masses of the two stellar populations are similar. They would thus expected to exhibit the same degree of segregation. However, it is unclear at what level rotational mixing would work for rapidly rotating stars. Rotational mixing would increase the core size of a rapidly rotating star, thus extending its MS lifetime compared with that of a non-rotating star of the same mass. If rotational mixing also plays a significant role in rapidly rotating stars in NGC 1856, then a less massive rapidly rotating star would have the same luminosity as a more massive non-rotating star, because the former has the same core size as the latter. In this paper, we have constrained our study of the two stellar components to the same magnitude range, which means that if rotational mixing is important for the red-component stars, their average mass should be smaller than that of the blue-component stars. In turn, this would lead to the former becoming less segregated than the blue stellar population.

It seems that rotational mixing *does* work for NGC 1856. Based on Figs 2 and 6, we can see these two populations of stars are not only different in color, but also in the loci of their MSTO points. The red sequence is characterized by a brighter turn-off point, indicating that stars belonging to the red MSTO region are more massive than stars associated with the blue MSTO region. This is presumably caused by the prolonged MS lifetime owing to rotational mixing. A promising method to evaluate the importance of rotational mixing for rapidly rotating stars is to measure the morphology of the SGBs in star clusters. If rotational mixing is negligible for rapidly rotating stars, then when stars evolve to the SGB stage, their rotation rates would quickly decrease because of the conservation of angular momentum. A coeval stellar population would then display a tight or converging SGB in its CMD. On the other hand, if rotational mixing is important, then a rapidly rotating star's core size would be permanently changed by the mixing effect before it evolved off the MS. In that case, the rapidly rotating stellar population would appear brighter than the slowly/non-rotating stellar population on both the MS and SGB, which would eventually produce a broadened SGB. Previous studies of intermediate-age clusters, which usually exhibit apparent eMSTO regions, have shown that the morphologies of their SGBs closely resemble or are consistent with simple stellar populations, indicating that for those clusters rotational mixing does not dramatically change the core sizes of the MSTO and SGB stars (Li et al. 2014a; Bastian et al. 2015; Li et al. 2016; Wu et al. 2016). However, this still needs to be explored for YMCs.

Finally, one may wonder why the stellar rotational distribution exhibits a dichotomy: 66% of the cluster's stellar population appear to be extremely rapid rotators, 34% are apparently non- or slowly rotating stars. Huang et al. (2010) studied spectra of more than 230 cluster and 370 field B-type stars. They found that most of their least-evolved, low-mass ($2M_{\odot} < M < 4M_{\odot}$) B-type stars are born as rapid rotators, while stars with rotation rates $\omega < 0.5$ compose 37% of the total population. Dufton et al. (2013) studied 334 stars of spectral types ranging from O9.5 to B3. They also found a bimodality in the distribution of the rotation rates of early B-type stars. Both studies are consistent with our results for NGC 1856. One explanation that may account for the two distinct populations in terms of the stellar rotation rates involves binary synchronization (see D'Antona et al. 2015, their Section 4.2). In the latter case, most slowly or non-rotating stars would be members of hard binary systems; the tidal interactions in such binary systems are thought to have slowed down the stars.

In summary, it seems that our results favor the rapid stellar rotation scenario rather than the multiple stellar populations model. However, more research of the importance of rotational mixing in rapidly rotating stars is required.

5. CONCLUSIONS

In this paper, we have studied the number ratio of stars belonging to two distinct components of NGC 1856's MS. We found a reliable number ratio of the blue and red MS components stars in NGC 1856 of 34%/66%. In addition, based on the adopted cluster number density center, both stellar components seem to be distributed homogeneously in space. Their cumulative number ratio remains constant over the entire radial range, and only a very weak dispersion appears in a narrow range for the annular number ratio profile.

We have discussed possible explanations on the basis of unresolved binary systems, multiple stellar populations, and rapid stellar rotation. We excluded the unresolved binaries as a cause. We confirmed that both multiple stellar populations and rapid stellar rotation can produce the observed features. However, most multiple stellar population scenarios have problems to explain the homogeneity of the radial distributions of the two observed stellar sequences. In addition, the enhanced metallicity that is needed in the multiple stellar population scenario would inevitably raise the 'mass budget problem' (Bastian et al. 2015). We emphasize that this conclusion is based on the assumption that NGC 1856 is representative of a young counterpart to the old GCs.

If the dominant effect caused by rapid stellar rotation is gravity darkening, then the observed MS bifurcation would favor the rapid stellar rotation scenario. However, currently no comprehensive studies have explored the relationship,

if any, between stellar rotation and their spatial distributions. In order to shed light on this issue, an improved understanding of the relative importance of rotational mixing for rapidly rotating stars is required.

We thank M. Di Criscienzo and F. D'Antona for providing us with the relevant isochrones. We acknowledge L. R. Bedin for his help with the *HST* footprints. CL is supported by the Macquarie Research Fellowship Scheme. CL, RdG and LD acknowledge financial support from the National Natural Science Foundation of China through grants 11373010, 11633005, and U1631102. APM acknowledges support from the Australian Research Council through a Discovery Early Career Researcher Award, DE150101816.

REFERENCES

Anderson, J., Sarajedini, A., Bedin, L. R., et al. 2008, AJ, 135, 2055
Bastian, N., & de Mink, S. E. 2009, MNRAS, 398, L11
Bastian, N., & Niederhofer, F. 2015, MNRAS, 448, 1863
Bastian, N., Cabrera-Ziri, I., & Salaris, M. 2015, MNRAS, 449, 3333
Bastian, N., Niederhofer, F., Kozhurina-Platais, V., et al. 2016, MNRAS,
Bekki, K., & Mackey, A. D. 2009, MNRAS, 394, 124
Bekki, K. 2011, MNRAS, 412, 2241
Brandt, T. D., & Huang, C. X. 2015, ApJ, 807, 25
Bressan, A., Marigo, P., Girardi, L., et al. 2012, MNRAS, 427, 127
Carretta, E., Bragaglia, A., Gratton, R. G., et al. 2009, A&A, 505, 117
Cassisi, S., Salaris, M., Pietrinferni, A., et al. 2008, ApJL, 672, L115
Correnti, M., Goudfrooij, P., Kalirai, J. S., et al. 2014, ApJ, 793, 121
Correnti, M., Goudfrooij, P., Puzia, T. H., & de Mink, S. E. 2015, MNRAS, 450, 3054
D'Antona, F., Di Criscienzo, M., Decressin, T., et al. 2015, MNRAS, 453, 2637
Decressin, T., Meynet, G., Charbonnel, C., Prantzos, N., & Ekström, S. 2007, A&A, 464, 1029
de Grijs, R., Li, C., Zheng, Y., et al. 2013, ApJ, 765, 4
de Mink, S. E., Pols, O. R., Langer, N., & Izzard, R. G. 2009, A&A, 507, L1
di Criscienzo, M., Ventura, P., D'Antona, F., Milone, A., & Piotto, G. 2010, MNRAS, 408, 999
Dieball, A., & Grebel, E. K. 2000, A&A, 358, 897
Dufton, P. L., Langer, N., Dunstall, P. R., et al. 2013, A&A, 550, A109
Ekström, S. et al., 2012, å, 537, A146
Georgiev, I. Y., Hilker, M., Puzia, T. H., Goudfrooij, P., & Baumgardt, H. 2009, MNRAS, 396, 1075
Georgy, C., Granada, A., Ekström, S., et al. 2014, A&A, 566, A21
Girardi, L., Goudfrooij, P., Kalirai, J. S., et al. 2013, MNRAS, 431, 3501
Goudfrooij, P., Girardi, L., Kozhurina-Platais, V., et al. 2014, ApJ, 797, 35
Goudfrooij, P., Girardi, L., Rosenfield, P., et al. 2015, MNRAS, 450, 1693
Hénault-Brunet, V., Gieles, M., Agertz, O., & Read, J. I. 2015, MNRAS, 450, 1164
Huang, W., Gies, D. R., & McSwain, M. V. 2010, ApJ, 722, 605
Khalaj, P., & Baumgardt, H. 2015, MNRAS, 452, 924
Kouwenhoven, M. B. N., Brown, A. G. A., Zinnecker, H., Kaper, L., & Portegies Zwart, S. F. 2005, A&A, 430, 137
Kouwenhoven, M. B. N., Brown, A. G. A., Portegies Zwart, S. F., & Kaper, L. 2007, A&A, 474, 77
Kraft, R. P. 1979, ARA&A, 17, 309
Lardo, C., Bellazzini, M., Pancino, E., et al. 2011, A&A, 525, A114
Larsen, S. S., Strader, J., & Brodie, J. P. 2012, A&A, 544, L14
Li, C., de Grijs, R., & Deng, L. 2013, MNRAS, 436, 1497
Li, C., de Grijs, R., & Deng, L. 2014, Nature, 516, 367
Li, C., de Grijs, R., Deng, L., et al. 2014, ApJ, 790, 35
Li, C., de Grijs, R., & Deng, L. 2016, RAA, in press (arXiv:1609.00894)
Li, C., de Grijs, R., Deng, L., et al. 2016, Nature, 529, 502
Li, C., de Grijs, R., Bastian, N., et al. 2016, MNRAS, 461, 3212
Lim, D., Lee, Y., Pasquato M., Han, S., & Roh D. 2016, ApJ, in press (arXiv: 1609.08174)
Longmore, S. N., Kruijssen, J. M. D., Bastian, N., et al. 2014, Protostars and Planets VI, 291
Marino, A. F., Milone, A. P., Piotto, G., et al. 2009, A&A, 505, 1099
Marino, A. F., Milone, A. P., Karakas, A. I., et al. 2015, MNRAS, 450, 815
Massari, D., Lapenna, E., Bragaglia, A., et al. 2016, MNRAS, in press (arXiv:1603.02827)
McLaughlin, D. E., & van der Marel, R. P. 2005, ApJS, 161, 304
Milone, A. P., Bedin, L. R., Piotto, G., & Anderson, J. 2009, A&A, 497, 755
Milone, A. P., Piotto, G., Bedin, L. R., et al. 2012, ApJ, 744, 58
Milone, A. P., Bedin, L. R., Piotto, G., et al. 2015, MNRAS, 450, 3750
Milone, A. P., Marino, A. F., Piotto, G., et al. 2015, ApJ, 808, 51
Milone, A. P., Marino, A. F., D'Antona, F., et al. 2016, MNRAS, 458, 4368
Nataf, D. M., Gould, A., Pinsonneault, M. H., & Stetson, P. B. 2011, ApJ, 736, 94
Niederhofer, F., Georgy, C., Bastian, N., & Ekström, S. 2015, MNRAS, 453, 2070
Niederhofer, F., Bastian, N., Kozhurina-Platais, V., et al. 2016, A&A, 586, A148
Piotto, G., Milone, A. P., Bedin, L. R., et al. 2015, AJ, 149, 91
Piotto, G., Milone, A. P., Bedin, L. R., et al. 2015, AJ, 149, 91
Rubele, S., Kerber, L., & Girardi, L. 2010, MNRAS, 403, 1156
Reggiani, M. M., & Meyer, M. R. 2011, ApJ, 738, 60
Renzini, A. 2008, MNRAS, 391, 354
Renzini, A., D'Antona, F., Cassisi, S., et al. 2015, MNRAS, 454, 4197
Rogers, H., & Pittard, J. M. 2013, MNRAS, 431, 1337
Vesperini, E., McMillan, S. L. W., D'Antona, F., & D'Ercole, A. 2013, MNRAS, 429, 1913
Ventura, P., & D'Antona, F. 2009, A&A, 499, 835
Werchan, F., & Zaritsky, D. 2011, AJ, 142, 48
Wu, X., Li, C., de Grijs, R., Deng, L. 2016, ApJL, 826, L14
Yang, W., Meng, X., Bi, S., et al. 2011, ApJL, 731, L37
Yang, W., Bi, S., Meng, X., & Liu, Z. 2013, ApJ, 776, 112